Synthesis of a rhodium(I) carbonyl complex with a chiral aminodiphosphine ligand and its immobilization onto aminopropyl functionalized silica gel

Pankaj Das[a]; Malabika Borah[a]; Chandan Sarmah[a]; Pradip K. Gogoi[a]; Lidia M. Alekseenko[b]; Svetlana M. Orlyk[b]

[a] Department of Chemistry, Dibrugarh University, Dibrugarh 786004, Assam, India [b] LV. Pisarzhevsky Institute of Physical Chemistry of NAS, Pr. Nauki 31, Kyiv 03028, Ukraine

PLEASE SCROLL DOWN FOR ARTICLE

Taylor & Francis
Taylor & Francis Group

Synthesis of a rhodium(I) carbonyl complex with a chiral aminodiphosphine ligand and its immobilization onto aminopropyl functionalized silica gel

PANKAJ DAS*†, MALABIKA BORAH†, CHANDAN SARMAH†,
PRADIP K. GOGOI†, LIDIA M. ALEKSEENKO‡
and SVETLANA M. ORLYK‡

†Department of Chemistry, Dibrugarh University, Dibrugarh 786004, Assam, India
‡LV. Pisarzhevsky Institute of Physical Chemistry of NAS,
Pr. Nauki 31, Kyiv 03028, Ukraine

The reaction of $[Rh(CO)_2(\mu\text{-}Cl)]_2$ with two molar equivalents of a chiral ligand, (*R*)-N,N-bis(2-diphenylphosphinoethyl)-1-phenylethylamine(PNP*) yield a mono-carbonyl complex, $[Rh(CO)Cl(\eta^2\text{-}P,P\text{-}PNP^*)]$ (**1**), in which the potentially tridentate PNP* ligand coordinates in a bidentate fashion through P,P bonding. The complex was characterized by elemental analysis, FAB mass, IR, UV-Vis, ^1H- and $^{31}P\{^1H\}$-NMR spectroscopy. Variable temperature (223–298 K) $^{31}P\{^1H\}$-,NMR spectra of **1** showed a mixture of *cis* and *trans* isomers in the solution with the *trans* predominating at room temperature and the *cis* at lower temperature. Complex **1** was immobilized on silica through axial coordination of amine from 3-aminopropyltriethoxysilane functionalized silica. The immobilized materials were characterized by elemental analysis (N_2), FTIR, DTA–TGA, N_2-adsorption, XRD, and SEM analysis.

Keywords: Rhodium(I) complex; Chiral PNP ligand; Variable temperature $^{31}P\{^1H\}$-NMR; Immobilization; Silica functionalization

1. Introduction

Organic transformations mediated by catalytic use of chiral platinum complexes in homogeneous phase have intensified from academic and industrial needs [1]. Most chiral catalysts are a combination of optically pure ligand and a metal in a particular oxidation state. Often, the activity of a specific metal species can be adjusted by varying the electronic and steric properties of the ligand. As tertiary phosphines are highly efficient in many catalytic reactions, there is a continuing effort to develop and design chiral phosphine-based catalysts for asymmetric synthesis [2–4]. Previous studies have demonstrated that the chelating phosphine ligands (e.g., BINAP and CHIRAPHOS) are more efficient in inducing asymmetric reaction than simple monodentate phosphines [5–8]. However, compared to simple diphosphine ligands, mixed donor

ligands bearing a soft and hard combination of donors in the same ligand framework (e.g., PO, PN, POP, and PNP) have an additional advantage because of their hemilabile behavior [9–11]. In fact, chiral P,O and P,N donor hemilabile ligands have been used in asymmetric catalysis [3, 12–15], e.g., Polo et al. [14] reported a Rh(I) complex with enantiomerically pure hydroxylated phosphine, (1S,2S,5R)-1-diphenylphosphino-methyl-2-isopropyl-5-methyl-cyclohexanol and its catalytic activity for hydroformyla-tion of olefin and Tsarev et al. [15] reported rhodium and palladium complexes with chiral P,N-bidentate ligands with the palladium complexes showing enantioselectivity up to 93% for asymmetric alkylation.

Although homogeneous catalysts, in many cases, are more active and selective, the separation and recovery of the catalysts from reaction solution are problematic. To overcome this problem, covalent anchorage of homogeneous complexes onto different insoluble supports [16, 17] were much focused. Silane-coupling reagents serve as a linker keeping the catalyst center away from the support material so that it behaves like a homogeneous catalyst. This methodology has been used for the immobilization of several rhodium [18–24] and ruthenium [25–29] complexes onto different mesoporous supports such as SiO_2 [18–21, 25], MCM-41 [22–24, 26, 27], SBA-15 [24, 28, 29], etc. One important criterion is that the support material should have some surface silanol (SiOH) groups for the condensation between the –SiOH and the alkoxy or chloro groups of silane-coupling reagent, affording a Si–O–Si covalent bond formation [16]. Among different supports, silica is a relatively low-cost and readily available material possessing surface-active silanol which has been used earlier for the immobilization of rhodium complexes [18–21]. By using organosilane-coupling reagents containing different ligand functionality such as $–NH_2$, $–PPh_2$, –SH, etc., some of these materials are excellent heterogeneous catalysts.

As part of our interests on organorhodium chemistry of hemilabile ligands [30, 31] and their use as homogeneous catalysts, herein, we report the synthesis and characterization of a Rh(I) carbonyl complex with a chiral ligand, (R)-N,N-bis(2-diphenylpho-sphinoethyl)-1-phenylethylamine(PNP*). To the best of our knowledge, there is no report of rhodium metal complexes with this PNP* ligand though there exist some reports with iridium [32] and platinum [33]. Complex **1** was immobilized onto silica through axial coordination of amine from 3-aminopropyltriethoxysilane (APTES) covalently bound to silica. The catalytic activities for asymmetric hydroformylation are in progress and the results will be published elsewhere.

2. Experimental

2.1. *Instrumentation*

Elemental analyses were recorded by using Elementar Vario EL III Carlo Erba 1108. IR spectra were recorded in KBr using a Shimadzu Prestige-21 FTIR spectrophotometer from 4000 to 400 cm^{-1}. UV spectra were recorded using a Shimadzu UV 1700-UV-Vis spectrophotometer in dichloromethane from 200 to 450 nm. ^{1}H- and ^{31}P{^{1}H}-NMR spectra were recorded in $CDCl_3$ operating at 300.13 and 121.50 MHz, respectively, on a Bruker 400 MHz spectrometer. FAB mass spectra were recorded on a JEOL SX 102/DA-6000 mass spectrometer using Argon/Xenon (6 kv, 10 mA) as the FAB gas.

The accelerating voltage was 10 kV and the spectra were recorded at room temperature. The matrix used was *m*-nitrobenzyl alcohol (NBA) whose peaks may appear at *m/z* = 136, 137, 154, 289, and 307 in the absence of any metal ions. If metal ions like Na ion are present, these peaks may be shifted. The X-ray powder diffraction patterns were recorded on a Bruker AXS D8 Advance fully automatic powder X-ray diffractometer with Cu-Kα (1.542 Å) radiation. The SEM images were recorded in a LEO 1430 VP scanning electron microscope. The DTA–TGA of the materials were recorded on a Perkin Elmer DTA–TGA instrument (Model: Pyris Diamond) under air at a heating rate of $10°C \, min^{-1}$.

The specific areas of the samples were determined from the argon thermal desorption (composition of work mixture: 5% Ar + 95% He) with GC control. Before this procedure, all samples were heated at 150°C.

2.2. *Materials*

Silica gel (100–200 mesh) was purchased from Merck and dehydrated by heating at 120°C for 2 h prior to use; APTES and [Rh(CO)$_2$Cl$_2$] were purchased from Aldrich. The ligand (*R*)-N,N-bis(2-diphenylphosphinoethyl)-1-phenylethylamine(PNP*) was purchased from Fluka. All other chemicals and solvents were purchased from different Indian firms. The solvents were distilled and dried prior to use. The reactions were performed under inert atmosphere. Rhodium analysis was performed by the standard literature method [34].

2.3. *Synthesis of [Rh(CO)Cl(η^2-P,P-PNP*)] (1)*

To a solution of [Rh(CO)$_2$Cl]$_2$ (0.1 g, 0.257 mmol) in 50 mL of dichloromethane, a solution of PNP* R(+)-N,N-bis(2-diphenylphosphinomethyl)-1-phenylethylamine (0.3 g, 0.55 mmol) in 30 mL of dichloromethane was added dropwise. The solution was stirred under continuous flow of nitrogen at room temperature for about 20 min, during which the color gradually changes from red to yellow-brown. The solvent was then evaporated and **1** was isolated from the residue by column chromatography using silica gel with acetone as an eluting solvent. After evaporation, **1** was isolated as a deep yellow (brown) solid. Yield: 86%. Anal. Calcd for C$_{37}$H$_{37}$NOP$_2$ClRh: C, 62.34; H, 5.20; N, 1.20. Found: C, 61.76; H, 5.09; N, 1.17. IR (KBr): 1965 cm^{-1} ν(CO), UV-Vis (CH$_2$Cl$_2$), λ_{max} (nm): 228, 274, and 360.

2.4. *Modification of silica surface*

Silica (2.0 g) was refluxed for 24 h with 3.8 mmol of APTES in 100 mL of dry toluene under nitrogen. After cooling, the solids were separated from the solvent by filtration and washed repeatedly through Soxhlet extraction with toluene. The materials were then dried at 120°C for 6 h and designated as SiO$_2$@APTES. Elemental analysis: N, 1.82%; specific surface area: $277.7 \, m^2 \, g^{-1}$ (free silica $351.7 \, m^2 \, g^{-1}$).

2.5. *Immobilized complex 1 onto SiO$_2$@APTES*

One gram of SiO$_2$@APTES was treated with 0.04 g of **1** in 40 mL of CH$_2$Cl$_2$ and the reaction mixture was refluxed under nitrogen for 3 h. The resulting solution was filtered and the light yellow solids were washed several times through Soxhlet extraction with CH$_2$Cl$_2$ until the physisorbed complexes were removed from the surfaces. The materials were designated as **1**@SiO$_2$-APTES. Elemental analysis: N, 2.02%; specific surface area: 242.0 m^2 g^{-1}.

3. Results and discussion

3.1. *Synthesis, elemental analysis, and mass spectra*

The chlorobridged dimer, [Rh(CO)$_2$Cl]$_2$, undergoes bridge splitting with two equivalents of PNP* to give a monocarbonyl complex, [Rh(CO)Cl(η^2-P,P-PNP*)] (**1**), where the potentially tridentate PNP* ligand binds bidentate through P,P. The elemental analysis and FAB mass spectra of **1** are consistent with the formulation. The fragmentation pattern of FAB mass spectrum of **1** is shown in "Supplementary material" (www.informaworld.com/GCOO). The base peak appears at $m/z = 676$ (100%) which corresponds to the [Rh(CO)(PNP*)] fragment formed by the removal of Cl$^-$ from the complex. The other peaks at m/z 647, 571, and 543 are due to gradual loss of carbonyl, phenyl, and –CH(Me) groups, respectively, from the base peak.

3.2. *FTIR spectra*

The IR spectrum of **1** in KBr shows one strong ν(CO) band at 1965 cm^{-1} consistent with square planar Rh(I) carbonyl complex. Such a low ν(CO) suggests high electron density on the Rh-center, consistent with coordination of PNP* through two P-atoms which donate electron density to the metal center [30]. The two P,P donors may occupy either mutual *trans* or *cis* positions. However, the ν(CO) value at 1965 cm^{-1} is very close to *trans*-[Rh(CO)Cl(PPh$_3$)$_2$] [35] and other *trans*-diphosphine complexes [36–38] shown in table 1, suggesting that the two P-donors of **1** are *trans*. Two phosphorus' *cis* ruled out as *cis*-diphosphine complexes show ν(CO) at a relatively higher wavenumber [39, 40]. IR spectra recorded in CHCl$_3$ show a very broad band centered at 1975 cm^{-1} along with a much less intense shoulder at 2010 cm^{-1}, suggesting a mixture of *cis* and *trans* isomers in solution. The major peak observed at about 1975 cm^{-1} is very close to the solid state ν(CO) value (1965 cm^{-1}), suggesting the predominant presence of *trans*-complex in the solution. Similar behavior was observed by Espinet *et al.* [41] for a Rh(I) monocarbonyl complex with an NPN ligand.

3.3. *UV-Vis spectra*

UV-Vis spectrum of **1** in dichloromethane shows two intense bands at 228 and 274 nm attributed to intraligand π–π* and n–π* transitions, respectively. Compared to free ligand (228 and 246 nm), the former band shows no shift, whereas the latter band shows a shift of 26 nm, indicating a change of electronic environment of the ligand due to

Table 1. Comparison of ν(CO) values of **1** with some reported *cis* and *trans* Rh(I) diphosphine complex.

Complex	ν(CO) (cm^{-1})	References
trans-[Rh(CO)Cl(η^2-P,P-PNP)]	1965	This work
trans-[Rh(CO)Cl(PPh$_3$)$_2$]	1964	[35]
trans-[Rh(CO)Cl{Ph$_2$PC$_6$H$_4$C(O)O(CH$_2$)$_2$OC(O)C$_6$H$_4$PPh$_2$}]	1965	[36]
trans-[Rh(CO)Cl{Ph$_2$PC$_6$H$_4$(CH$_2$)$_2$C$_6$H$_4$PPh$_2$}]	1970	[37]
trans-[Rh(CO)Cl(4-Ph$_2$PC$_6$H$_4$COOMe)$_2$]	1977	[30]
trans-[Rh(CO)Cl{Ph$_2$PC$_6$H$_4$C(O)NPh(CH$_2$)$_2$OC(O)C$_6$H$_4$PPh$_2$}]	1971	[38]
cis-[Rh(CO)Cl(PPh$_3$)$_2$]	2010	[39]
cis-[Rh(CO)Cl(PPh$_2$CH$_2$CH$_2$PPh$_2$)]	2011	[40]
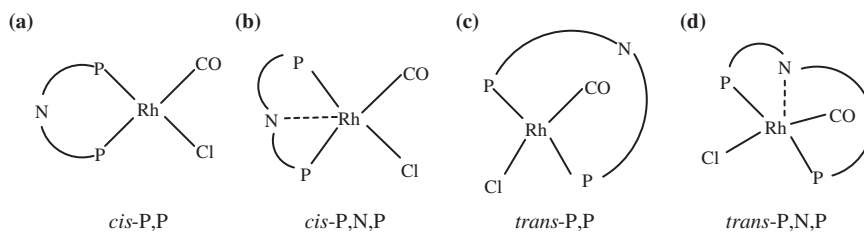
Figure 1. Possible isomeric structures of **1**.

complexation. In addition to intraligand bands, **1** also shows a band at 360 nm, which could be assigned to metal-to-ligand charge transfer [42].

3.4. $^{31}P\{^1H\}$- and ^1H-NMR spectra

Complex **1** has four possible isomeric structures shown in figure 1. The ^{31}P{^{1}H}-NMR spectra of **1** in CDCl$_3$ solution at room temperature show multiple signals in the range 20–62 ppm, indicating the presence of more than one isomer in the solution, consistent with the complicated stereochemistry of some reported hemilabile ligands [9, 10]. The *cis* diphosphine isomer (**1a**) is expected to give an ABX spin system (A=B=P and X=Rh) as the two P-atoms of the PP chelate are not equivalent, while the *trans* isomer (**1c**) is expected to give an AX spin system (A for two equivalent P atoms and X for Rh). The ^{31}P-NMR spectrum of **1** shows both AX and ABX pattern of bands in an approximate ratio of 3 : 2 assigned to *trans* and *cis* isomers, respectively, indicating the presence of both *trans* and *cis* isomers in the solution. The major set of signal shows a doublet at δ 21 ppm and a coupling constant of J_{RhP} 123 Hz, consistent with the *trans* isomer, while the minor set shows two doublets of doublets at δ 43 ppm with corresponding coupling constants $J_{RhP} \approx 141$ and $J_{PP} \approx 45$ Hz, indicating *cis*-coordination of phosphorus. In addition to ABX and AX signals, the ^{31}P{^{1}H}-NMR spectra at 298 K show two other signals, one broad singlet at 62 ppm and another at 32 ppm. These additional resonances may possibly be due to an alternative *cis* P,N,P (isomer **1b**) and *trans* P,N,P (isomer **1d**) coordination mode, as it is anticipated that coordination through P,N,P would further bring the ^{31}P signal downfield compared to P,P bonding [32]. PNP* while coordinated with iridium [32] and platinum [33] binds both bidentate

(with P,P bonding) and/or tridentate (with P,N,P bonding) and while bidentate, prefers to coordinate through P,P in a *cis* position. In order to study the fluxional behavior, a variable temperature (223–298 K) $^{31}P\{^{1}H\}$-NMR experiment was performed (figure 2). On lowering the temperature from 298 to 223 K, a gradual decrease in the

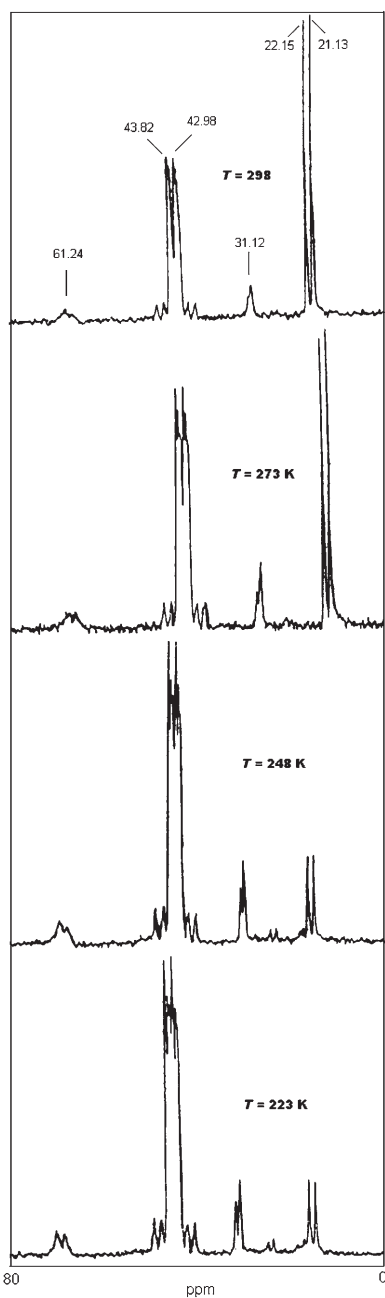Figure 2. Variable temperature (223–298 K) $^{31}P\{^{1}H\}$-NMR spectra of **1** recorded in CDCl$_3$ with reference to 85% H$_3$PO$_4$.

intensity of the AX spectrum at 21 ppm and an increase in the intensity of the ABX spectrum at 43 ppm was observed. Thus, at 223 K, the *cis* isomer **1c** is the most stable and at 298 K, the *trans* isomer **1a** is the most stable. Though the mechanism of this inter-conversion between *cis* and *trans* isomer is not clear, a possible involvement of *cis*-P,N,P (figure 1b) and *trans*-P,N,P bonding (figure 1d) in the exchange process could not be ruled out; the reversible coordination of N-donor (switching from P,N,P to P,P mode) to Rh(I) is most likely responsible for the equilibration in the solution. The broad singlet at 62 ppm and sharp singlet at 32 ppm at 298 K proposed for the *cis* and *trans* P,N,P bonding changed to a broad doublet and a sharp doublet at 223 K. The ^{1}H-NMR spectrum of **1** shows multiplets at δ 7.0–9.0 ppm due to aromatic protons present in the complex. Compared to free ligand, these values shift slightly downfield indicating coordination through phosphorus. Peaks for the aliphatic protons, i.e., –CH, –CH$_2$, and –CH$_3$, appear as indistinguishable multiplets consistent with the presence of several isomeric structures in the solution, and the spectra cannot be interpreted exactly.

3.5. *Immobilization of 1 onto silica*

The modification of silica surface through surface functionalization with APTES and immobilization of **1** onto modified silica was done following a strategy shown in scheme 1. On the basis of nitrogen elemental analysis, the amount of APTES anchored onto silica was determined as 1.30 mmol g^{-1}. The amount of complex immobilized into SiO$_2$@APTES was 5.7 μmol g^{-1}, determined from rhodium analysis. The specific surface area obtained by N$_2$-desorption analysis for free silica was 351.7 m^2 g^{-1}, which upon functionalization with APTES decreases to 277.7 m^2 g^{-1}. A further decrease in the surface area was obtained for **1**@SiO$_2$-APTES (242 m^2 g^{-1}) compared to SiO$_2$@APTES, consistent with immobilization of the complex onto silica.

3.5.1. IR spectral characterization. The FTIR spectra of free silica, APTES functionalized silica (SiO$_2$@APTES), and complex immobilized silica (**1**@SiO$_2$-APTES) are shown in "Supplementary material." The spectrum of free silica exhibits two broad bands, –OH stretching frequencies at 3616 and 3543 cm^{-1} due to the
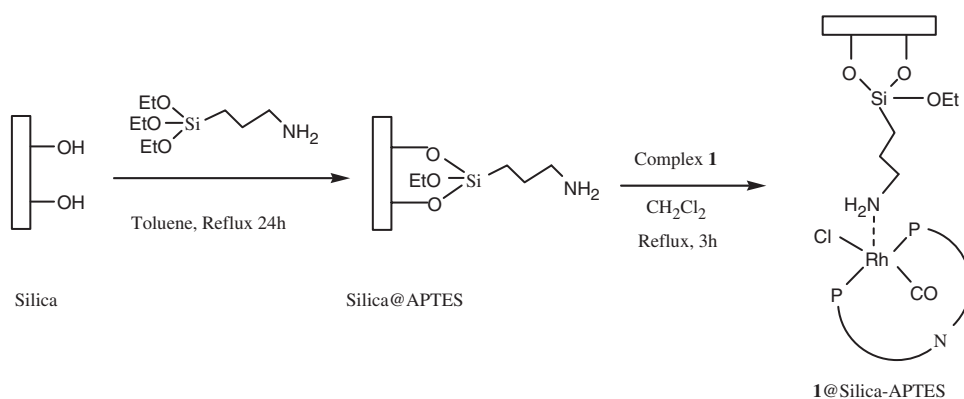
Scheme 1. Immobilization of **1** onto 3-aminopropyltriethoxysilane (APTES) functionalized silica gel.

presence of Si–OH and water physically associated with silica surface. The spectrum also shows a broad peak at $3240\,cm^{-1}$ due to hydrogen bonded –OH. Upon functionalization of silica with APTES, the intensity of the broad band around $3600\,cm^{-1}$ decreases, indicating successful grafting of the organosilane with silica surface *via* Si–O–Si bond formation [43]. In addition, SiO_2@APTES also shows the characteristics bands for CH and NH stretching from 2800 to $3200\,cm^{-1}$. Upon immobilization of the rhodium carbonyl complex onto SiO_2@APTES, there is no significant change in the FTIR spectrum as the quantity of metal complex immobilized was so low that its absorption peaks were masked by the strong background peaks of silica-APTES matrix. The only difference noticed between SiO_2@APTES and **1**@SiO_2-APTES spectra is the appearance of a low-intensity band at $1979\,cm^{-1}$ due to the
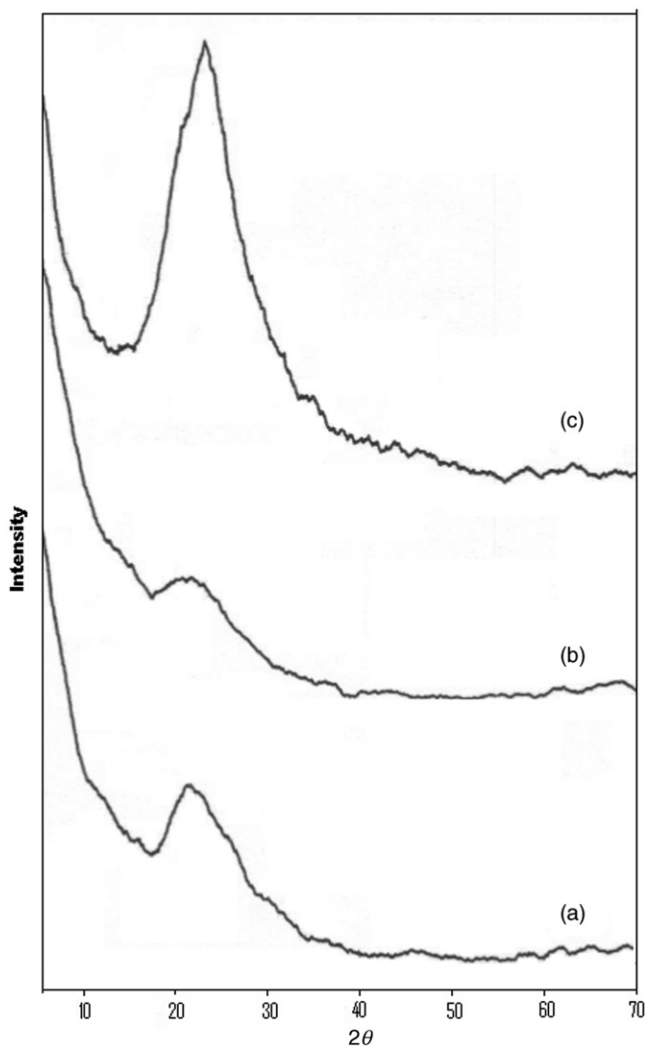
Figure 3. XRD patterns of (a) free silica gel, (b) SiO_2@APTES, and (c) **1**@SiO_2-APTES.

presence of the carbonyl group in accordance with the immobilization of the Rh-complex onto the functionalized silica; shift about $14\,cm^{-1}$ higher clearly indicates the interaction between the support and metal center.

3.5.2. XRD and SEM analysis. The XRD spectrum (figure 3) of unfunctionalized silica exhibits a broad halo with center at $2\theta = 20.01°$ with corresponding d-spacing of $4.44\,\text{Å}$. Upon silylation of silica with APTES, the resulting material, SiO_2@APTES,
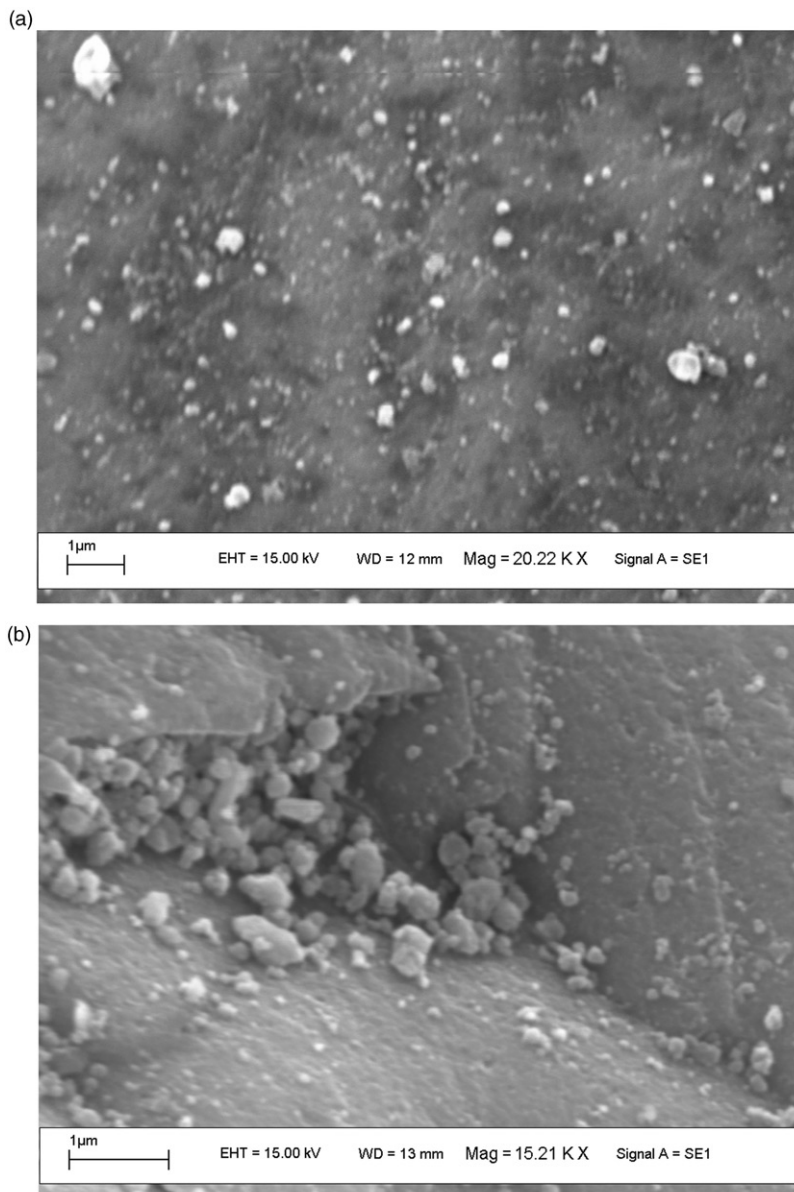

(a)

1µm   EHT = 15.00 kV   WD = 12 mm   Mag = 20.22 K X   Signal A = SE1

(b)

1µm   EHT = 15.00 kV   WD = 13 mm   Mag = 15.21 K X   Signal A = SE1

Figure 4.   SEM image of (a) SiO_2@APTES and (b) **1**@SiO_2-APTES.

shows a very negligible shift in the 2θ value but displays a slight decrease in halo intensity. However, upon immobilization of the rhodium complex on SiO_2@APTES, the resulting material, **1**@SiO_2-APTES, shows a marginal shift in the center of halo position ($2\theta = 21.85°$) and an increase in the intensity. Since the change in halo positions are not prominent between the parent silica, SiO_2@APTES and **1**@SiO_2-APTES, it could be concluded that the textural properties of the support are not destroyed during the grafting (only decreasing of surface area). The phase of rhodium complex is absent in the immobilized sample. The change in intensities indicates some increase in the degree of ordering of the structure (by rhodium presence) of the silica matrix upon immobilization, which is also corroborated by the SEM analysis. Figure 4(a) and (b) shows the SEM images of SiO_2@APTES and **1**@SiO_2-APTES, respectively. Figure 4(b) shows that the metal particles are sparsely attached to the silica surface (separated by white patches), which is inhomogeneous and are of wide particle size distribution.

3.5.3. TGA analysis. The TGA weight loss pattern of the parent silica material shows only one peak with a corresponding weight loss of about 12% in the region 40–150°C attributed to the loss of physisorbed water and the surface hydroxyl present in silica. In addition to the loss of physisorbed water in the range 40–142°C, the APTES functionalized silica, SiO_2@APTES, also displays other successive weight losses (8.27%) without clearly distinct steps in the region 236–611°C attributable to the loss of organic functionalities attached to the APTES unit. Based on DTA–TGA weight loss, the amount of APTES loaded onto silica surface was calculated as 1.18 mmol g^{-1}, which is slightly less than that determined by N elemental analysis. TGA analysis of **1** shows that the major weight loss starts at *ca* 198°C and continues till *ca* 612°C with several inflections observed by DTA attributed to the gradual loss of organic functionalities from the ligand. However, upon immobilization of the complex onto silica, the decomposition of organic functionality starts at *ca* 333°C and continues up to *ca* 750°C. Compared to the free complex, the immobilized complex shows higher decomposition temperature consistent with the interaction of the support with the metal center.

4. Conclusions

A rhodium(I) carbonyl complex with a chiral aminodiphosphine ligand was synthesized; the potentially tridentate PNP ligand coordinates bidentate through P,P. Variable temperature $^{31}P\{^1H\}$-NMR spectra of the complex suggest several isomeric structures in the solution; at room temperature, the *trans* isomer dominates, whereas at lower temperature *cis* dominates. The complex was immobilized onto silica through axial coordination of amine from APTES covalently bound to silica.

References

[1] T.T.L. Au-Yeung, A.S.C. Chan. *Coord. Chem. Rev.*, **248**, 2151 (2004).
[2] G. Erre, S. Enthaler, K. Junge, S. Gladiali, M. Beller. *Coord. Chem. Rev.*, **252**, 471 (2008).
[3] W. Tang, X. Zhang. *Chem. Rev.*, **103**, 3029 (2003).
[4] A.G. Hu, H.L. Ngo, W. Lin. *Angew. Chem. Int. Ed.*, **43**, 2501 (2004).
[5] G.Y. Zhou, X. Zhang. *Chem. Commun.*, 1124 (2002).
[6] G.Y. Zhou, W. Tang, W.B. Wang, L. Li, X. Zhang. *J. Am. Chem. Soc.*, **124**, 4952 (2002).
[7] J. Wassenaar, J.N.H. Reek. *Dalton Trans.*, 3750 (2007).
[8] R. Hoen, J.A.F. Boogers, H. Bernsmann, A.J. Minnaard, A. Meetsma, T.D.T. Wegman, A.H.M. de Vries, J.G. de Vries, B.L. Feringa. *Angew. Chem. Int. Ed.*, **44**, 4209 (2005).
[9] A. Bader, E. Lindner. *Coord. Chem. Rev.*, **108**, 27 (1991).
[10] P. Espinet, K. Soulantica. *Coord. Chem. Rev.*, **193–195**, 499 (1999).
[11] P. Braunstein, F. Naud. *Angew. Chem. Int. Ed.*, **40**, 680 (2001).
[12] I.D. Kostas, K.A. Vallianatou, J. Holtz, A. Borner. *Appl. Organomet. Chem.*, **19**, 1090 (2005).
[13] J.L. Bookham, D.M. Smithies, M.T. Pett. *J. Chem. Soc., Dalton Trans.*, 975 (2000).
[14] J. Duran, D. Oliver, A. Polo, J. Real, J. Benet-Buchholz, X. Fontrodona. *Tetrahedron: Asymmetry*, **14**, 2529 (2003).
[15] K.N. Gavrilov, V.N. Tsarev, S.I. Konkin, S.E. Lyubimov, A.A. Korlyukov, M.Y. Antipin, V.A. Davankov. *Eur. J. Inorg. Chem.*, 3311 (2005).
[16] A. Corma, H. Garcia. *Adv. Synth. Catal.*, **348**, 1391 (2006).
[17] P. Das, A.R. Silva, A.P. Carvalho, J. Pires, C. Freire. *Catal. Lett.*, **44**, 2865 (2009).
[18] C.M. Standfest-Hauser, T. Lummerstorfer, R. Schmid, H. Hoffmann, K. Kirchner, M. Puchberger, A.M. Trzeciak, E. Mieczynska, W. Tylus, J.J. Ziolkowski. *J. Mol. Catal. A: Chem.*, **210**, 179 (2004).
[19] Z.M. Michalska, L. Rogalski, K. Rozga-Wijas, J. Chojnowski, W. Fortuniak, M. Scibiorek. *J. Mol. Catal. A: Chem.*, **208**, 187 (2004).
[20] L. Huang, S. Kawl. *J. Mol. Catal. A: Chem.*, **211**, 23 (2004).
[21] H. Gao, R.J. Angelici. *J. Mol. Catal. A: Chem.*, **145**, 83 (1999).
[22] H. Balcar, J.C. Čejka, J. Sedláček, J. Svoboda, J. Zednik, Z. Bastl, V. Bosáček, J. Vohlidal. *J. Mol. Catal. A: Chem.*, **203**, 287 (2003).
[23] W. Zhou, D. He. *Catal. Lett.*, **127**, 437 (2009).
[24] A. Crosman, W.F. Hoelderich. *Catal. Today*, **121**, 130 (2007).
[25] F.G. Doro, U.P. Rodrigues-Filho, E. Tfouni. *J. Colloid Interface Sci.*, **307**, 405 (2007).
[26] T. Soundiressane, S. Selvakumar, S. Ménage, O. Hamelin, M. Fontecave, A.P. Singh. *J. Mol. Catal. A: Chem.*, **270**, 132 (2007).
[27] T. Joseph, S.S. Deshpande, S.B. Halligudi, A. Vinu, S. Ernst, M. Hartmann. *J. Mol. Catal. A: Chem.*, **206**, 13 (2003).
[28] S. Syukri, A. Sakthivel, W. Sun, F.E. Kuhn. *Catal. Lett.*, **128**, 18 (2009).
[29] S. Sahoo, P. Kumar, F. Lefebvre, S.B. Halligudi. *J. Mol. Catal. A: Chem.*, **273**, 102 (2007).
[30] D.K. Dutta, J.D. Woollins, A.M.Z. Slawin, D. Konwar, P. Das, M. Sharma, P. Bhattacharyya, S.M. Aucott. *Dalton Trans.*, 2674 (2003).
[31] P. Das, M. Sharma, N. Kumari, D. Konwar, D.K. Dutta. *Appl. Organomet. Chem.*, **16**, 302 (2002).
[32] C. Bianchini, E. Farnetti, L. Glendenning, M. Graziani, J.G. Nardin, M. Peruzzini, E. Rocchini, F. Zanobini. *Organometallics*, **14**, 1489 (1995).
[33] L. Janosi, T. Kegl, L. Hajba, Z. Berente, L. Kollar. *Inorg. Chim. Acta*, **316**, 135 (2001).
[34] P.K. Gogoi. Magnetic and spectral studies on dithiophosphate and dithiophosphinates of some first row transition and light platinum metals. PhD thesis, Indian Institute of Technology, Bombay (1981).
[35] J. Chatt, B.L. Shaw. *J. Chem. Soc. A*, 1437 (1966).
[36] P. Stepnicka, I. Cisarova. *J. Chem. Soc., Dalton Trans.*, 2807 (1998).
[37] M.A. Bennett, R.N. Johnson, I.B. Tomkins. *J. Organomet. Chem.*, **128**, 73 (1977).
[38] C. Lambert, G. Noll. *Chem. Eur. J.*, **8**, 3467 (2002).
[39] A.R. Sanger. *J. Chem. Soc., Chem. Commun.*, 893 (1975).
[40] L. Gonsalvi, H. Adams, G.J. Sunley, E. Ditzel, A. Haynes. *J. Am. Chem. Soc.*, **124**, 13597 (2002).
[41] M.A. Alonso, J.A. Casares, P. Espinet, K. Soulantica. *Inorg. Chem.*, **39**, 705 (2000).
[42] K. Wajda-Hermanowicz, Z. Ciunik, A. Kochel. *Inorg. Chem.*, **45**, 3369 (2006).
[43] I.K. Biernacka, A.R. Silva, A.P. Carvalho, J. Pires, C. Freire. *Langmuir*, **21**, 10825 (2005).